JOURNAL OF MATERIALS SCIENCE 33 (1998) 5557–5568

Processing and microstructural characterisation of RBSiC-$TaSi_2$ composites

S. P. SIMNER*, P. XIAO†, B. DERBY
Department of Materials Science and Engineering, University of Oxford, Parks Road OX1 3PH, United Kingdom

Reaction bonded silicon carbide (RBSiC) ceramics typically contain 10 vol% silicon inherent to the reaction bonding process. However, the relatively low melting point (1410 °C) of the silicon phase is a limiting factor in the high temperature use of RBSiC materials. The application temperature can potentially be enhanced by replacing the silicon with more refractory metal disilicide phases. In this paper we report the infiltration of SiC-graphite compacts with alloyed Si-Ta melts in an attempt to precipitate $TaSi_2$ ($T_m = 2040$ °C) in place of the residual silicon. High density RBSiC-$TaSi_2$ ceramics with virtually no porosity were readily produced, but subsequent XRD and SEM examination revealed that the silicon phase was not completely removed. In addition, the materials possessed complex, inhomogeneous microstructures and were susceptible to various types of crack formation phenomena.

1. Introduction

Silicon carbide has long been considered a highly advanced engineering material exhibiting exceptional stability, strength and corrosion resistance at elevated temperatures. However, the sintering of SiC powders for the bulk fabrication of high density ceramics is very difficult. As with many other covalently bonded compounds, SiC exhibits low vacancy diffusion, and normal sintering is strongly inhibited. Additives and the use of high temperatures may be employed to aid the sintering process. Pressureless solid state sintering is possible at temperatures of 1900–2100 °C with small amounts (<1 vol %) of boron and carbon dopants. However, SiC ceramics of near theoretical densities can only be produced by hot pressing, which requires temperatures approaching 2000 °C, pressures greater than 30 MPa, and the use of boron carbide (1–5 vol %) and alumina (3–5 vol %) dopant materials.

An alternative SiC bulk processing technique is reaction bonding. Reaction bonded SiC (RBSiC) was first developed in the 1950s by Popper [1] as a nuclear fuel cladding material, and is now produced via two highly developed commercial processes: the REFEL SiC [2], and the Ford KT SiC [3] processes. Advantages over conventional sintering techniques include lower processing temperatures (∼1500 °C as opposed to ∼2000 °C), shorter processing times and minimal shape and dimensional changes from the original preform.

The reaction bonding process involves the infiltration of a porous green compact of silicon carbide (α-SiC) and unreacted carbon with liquid silicon by a capillary action process [4]. An in situ reaction occurs between the silicon and the carbon to produce a secondary β-SiC phase, which then bonds the original SiC particles to produce a body of near theoretical density. The green body must incorporate sufficient porosity before firing to accommodate the formation of the "new" SiC on infiltration. The volume is approximately doubled as the carbon reacts to form SiC. In practice, approximately 10 vol % additional porosity, over that required to allow for volume expansion effects, is needed to prevent the formation of an impenetrable skin of β-SiC at the edges of the preform and thus to ensure complete silicon impregnation. After completion of the reaction the excess porosity remaining within the material is filled by silicon from the melt, referred to as the free or residual silicon phase [4]. The presence of this silicon phase limits the high temperature application of RBSiC materials. The low temperature properties of RBSiC are comparable to HPSiC, but the high temperature properties and applications are reduced due to the relatively low melting point of silicon (1410 °C). The properties, microstructure and infiltration kinetics of RBSiC materials have been discussed in detail elsewhere [5–10].

In recent years, methods of replacing the silicon with more refractory metal disilicides have been investigated. Particular interest has been given to molybdenum disilicide ($MoSi_2$), which has a melting temperature of 2030 °C and exhibits excellent high temperature oxidation resistance and ductility [11]. Messner and Chiang [12–14] used alloyed Si-Mo melts in place of pure Si to infiltrate the green compact. Upon infiltration, Si from the melt reacts with the graphite in the compact to produce the secondary β-SiC phase. Consequently the

* *Present address:* Materials Sciences Department, Pacific Northwest National Laboratory, Richland, Washington 99352, USA.
† *Present address:* Department of Material Engineering, Brunel University, Uxbridge UB8 3PH, UK.

alloyed melt becomes depleted in Si and enriched in Mo, which eventually causes precipitation of an $MoSi_2$ phase into the porous regions of the preform.

Using this technique the correct melt concentration is essential. There must be enough silicon to react with the carbon in the preform and sufficient remaining to combine with Mo to precipitate the $MoSi_2$ phase. Once the melt concentration has been established, it is then possible to refer to the Mo-Si phase diagram to calculate the optimum infiltration temperature within the single phase liquid field. The temperature should be kept sufficiently above the liquidus, typically 50–100 °C, to prevent premature precipitation of the metal disilicide and incomplete infiltration and reaction. Infiltrating with melt concentrations between 4–8 mol % Mo, Messner and Chiang [13] were able to produce RBSiC-$MoSi_2$ composites of >90 % theoretical density with no detectable residual silicon or unreacted graphite. The $MoSi_2$ phase was also found to be homogeneously dispersed, and would therefore be expected to act as a good high temperature toughening phase due to its brittle-ductile transformation.

Similar work with alloyed melt systems has also been conducted by other researchers. Schmid *et al.* [15] used Si-Mo melts, but their studies indicated the continued existence of silicon in the composite and a poor distribution of $MoSi_2$. More recently, work by Singh [16] employed the use of Si-5 mol % Nb melts to produce RBSiC-$NbSi_2$ composite materials ($NbSi_2$ melting temperature = 1950 °C). However, XRD analysis indicated only partial silicon replacement with $NbSi_2$ and the materials exhibited a reduction in flexural strength as the temperature approached the melting point of silicon, as observed in "conventional" RBSiC ceramics.

In this work we have studied the use of Si-Ta melts to precipitate $TaSi_2$ in place of the detrimental silicon phase. This was undertaken to determine the universality of this processing technique, and to comprehensively study the microstructure of the materials produced. This alloy system satisfies the critical requirement of a binary eutectic composition between the silicide and silicon with a wide single phase liquid field. $TaSi_2$ has a melting temperature of 2040 °C, virtually equal to $MoSi_2$, and like $MoSi_2$ it exhibits a brittle-ductile transition around 1000 °C through the activation of "superlattice" dislocations, which provide additional slip and improved ductility [17]. As such, it might be expected to enhance the high temperature properties of the RBSiC materials.

2. Experimental

2.1. Green body forming

All green powder mixes were prepared using either F500 or F600 starter SiC materials supplied by Washington Mills Electro Minerals Ltd. (Manchester, UK). The as-supplied particle sizes of these starter powders are shown in Table I. Graphite was supplied by Aldrich Chemical Co. (Gillingham, UK) and the average particle size of the material was listed as 1–2 μm. Polyethylene glycol (PEG) with an average molecular weight (M_W) of 300 grams was used as the green compact binder material. The starter materials (α-SiC, graphite and PEG binder) were simply added together with water and a small amount of DISPEX A40 dispersant, a salt of a polycarboxylic acid supplied by Allied Colloids (Bradford, UK), to evenly disperse the graphite and SiC and to prevent particle agglomeration, and then ball milled for 12 hours with zirconia milling media. To achieve a homogeneous carbon density in the green compact, it is essential to produce a mix in which the graphite is uniformly dispersed. The powder mixes were freeze-dried, screened through a 0.5 mm sieve to break any large powder agglomerates, and then uniaxially cold pressed in a hardened steel die of 2.0 cm diameter using pressures between 50–150 MPa. All compacts were prepared using 30 wt % graphite and had theoretical green densities ranging between 1.70–1.75 g/cm^3. Typical compact dimensions were 2.0 cm diameter by ~0.5–1.5 cm height.

TABLE I Silicon carbide particle sizes used for green body preparation

Grit size Nomenclature	Maximum particle diameter (μm)	Median particle diameter (μm)	Minimum particle diameter (μm)
F500	25	12.8 ± 1.0	5
F600	19	9.3 ± 1.0	3

2.2. Alloyed melt preparation and the infiltration process

The melts were prepared by simply dry mixing the required proportions of Si and Ta powders (99.9 % purity, Aldrich UK). The mass and composition of the melt can be determined if we know the mass of graphite and the initial pore volume in the green compact. First, we can calculate the mass of Si required to react with the known mass of graphite. In addition, the formation of β-SiC on Si + C reaction will reduce the original pore volume in the sample, and if we know the new pore volume then it is possible to calculate the mass of $TaSi_2$ required to completely fill it. Hence the total melt mass will be the mass of Si needed to react with the graphite in the green compact plus the mass of $TaSi_2$ required to fill any porosity in the sample after the Si + C reaction has taken place. The masses of Si (M_{Si}) and Ta (M_{Ta}) required, and hence the melt composition, can be calculated from Equations 1 and 2 [18]. To simplify the equations, two assumptions have been made. First, that the compact volume remains constant before and after infiltration, and second, that the densities of the original α-SiC and the newly formed β-SiC are approximately equal.

$$M_{Si} = 2\left[\frac{\rho_{TaSi_2} \cdot MW_{Si}}{MW_{TaSi_2}}\right]\left[V_o - \frac{1}{\rho_{SiC}}\left(m_{\alpha-SiC} + m_C + m_C \cdot \frac{MW_{Si}}{MW_C}\right)\right] + m_C \cdot \frac{MW_{Si}}{MW_C} \quad (1)$$

$$M_{Ta} = \rho_{TaSi_2}\left[1 - \frac{2MW_{Si}}{MW_{TaSi_2}}\right]\left[V_o - \frac{1}{\rho_{SiC}}\left(m_{\alpha-SiC} + m_C + m_C \cdot \frac{MW_{Si}}{MW_C}\right)\right] \quad (2)$$

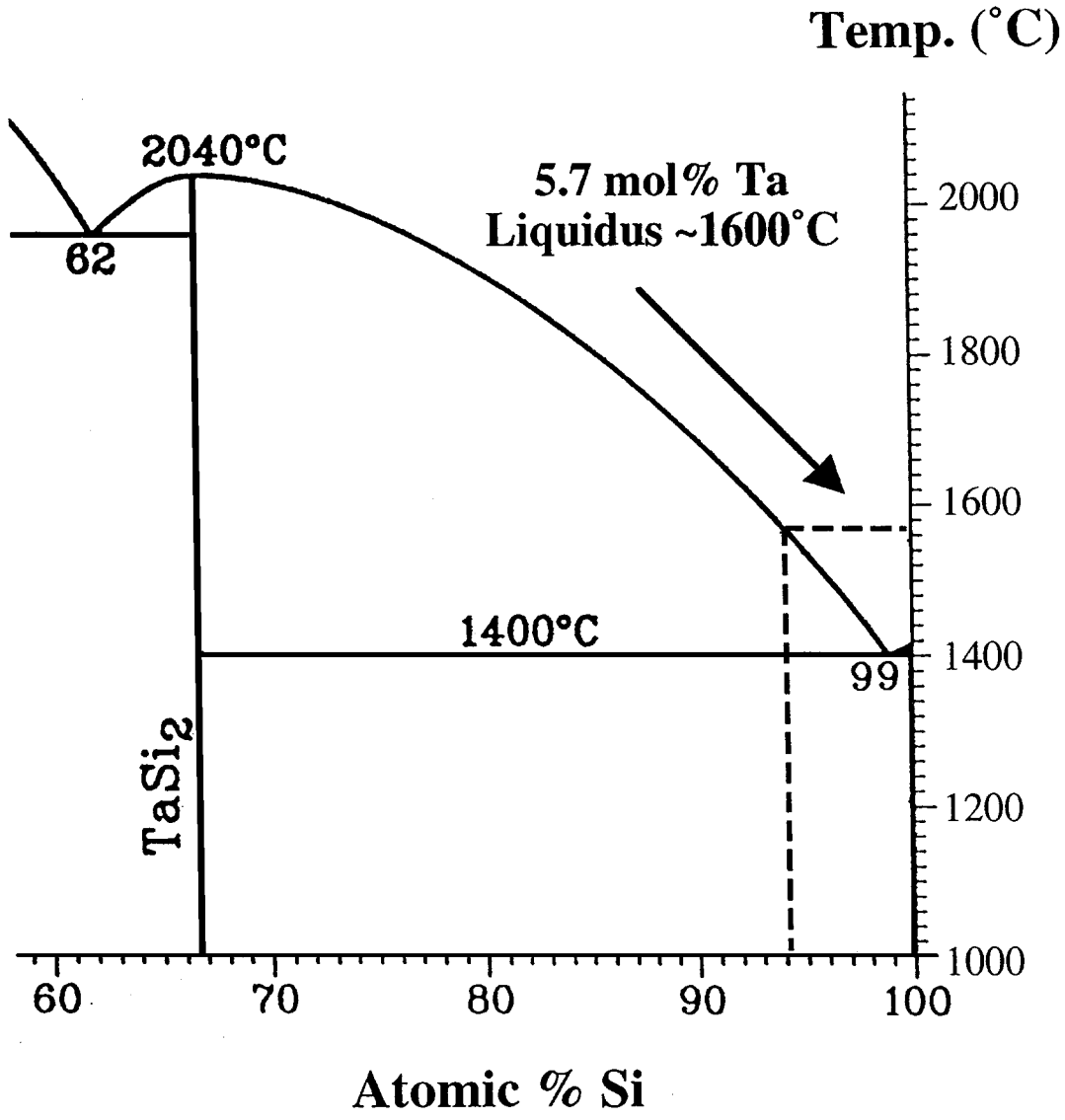

Figure 1 Relevant section of the Si-Ta phase diagram indicating the liquidus temperature for a melt composition of Si-5.7 mol % Ta (28 wt % Ta).

where

MW_{Si} = the molecular weight of silicon (28.01 g/mol)
MW_C = the molecular weight of carbon (12.01 g/mol)
MW_{TaSi_2} = the molecular weight of tantalum disilicide (236.97 g/mol)
ρ_{SiC} = the theoretical density of silicon carbide (3.21 g/cm^3)
ρ_{TaSi_2} = the theoretical density of tantalum disilicide (9.14 g/cm^3)
V_o = the volume of the green compact before firing
$m_{\alpha-SiC}$ = the mass of starter SiC in the green compact
m_C = the mass of graphite in the green compact

For a green compact with an original volume of 1.15 cm^3 and graphite content of 0.6 g, the alloyed melt composition and total melt mass were established at Si-28 wt % Ta (Si-5.7 mol % Ta) and 2.22 g, respectively.

The alloyed melt was initially loaded into a graphite crucible which was to be heated inductively. The green compact was placed over the crucible well but actually separated from the melt by a few millimetres. The reason for this set-up is to retard the initial rate of infiltration into the preform, as will be explained in greater detail in the next section.

The temperature of infiltration is determined by the composition of the melt and reference to the relevant section of the Si-Ta phase diagram [19], shown in Fig. 1. The liquidus temperature for a 28 wt % Ta melt is approximately 1600 °C. However, work by Messner [13] had suggested that the actual infiltration temperature should be at least 50–100 °C above the liquidus to prevent premature precipitation of the refractory disilicide and incomplete infiltration. Consequently, the infiltration temperature was set at 1700 °C. An optimised infiltration schedule is shown in Fig. 2. An initial heating rate of 2 °C/min up to 600 °C was required to burn off the PEG binder. Heating rates faster than this caused cracking of the uninfiltrated preforms as the binder evaporated too quickly. To ensure complete binder removal the furnace was held at 600 °C for 1 hour. This initial stage of processing was conducted under a coarse

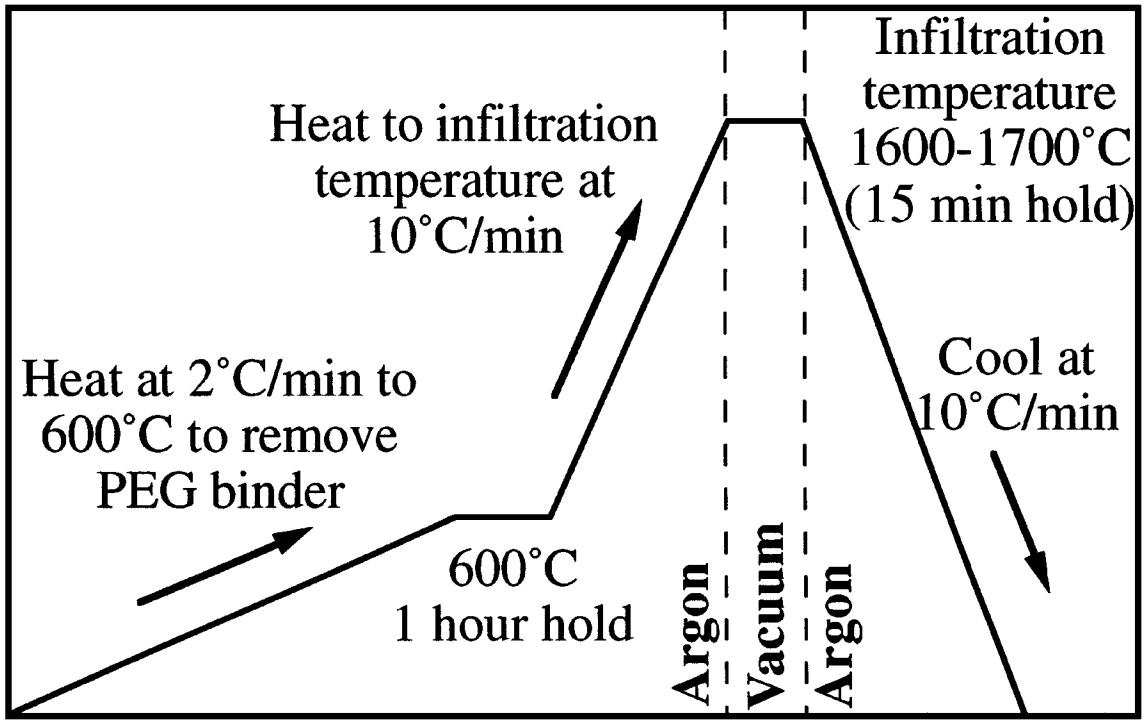

Figure 2 Optimised time-temperature schedule for alloyed Si-Ta melt infiltrations.

vacuum (∼2–3 mbar). Having removed the PEG, the heating rate was increased to 10 °C/min up to the infiltration temperature (∼1700 °C). For this stage of the schedule the furnace was back-filled with argon to a pressure of 1 bar, to reduce evaporation of the silicon in the melt prior to infiltration. At the desired infiltration temperature the chamber was evacuated to a coarse vacuum of 2 mbar ($\sim 2 \times 10^{-3}$ atm) which was found to significantly aid the melt penetration of the green compact. The furnace was left at the infiltration temperature for 15 minutes, to ensure that the Si + C reaction had gone to completion. After the 15 minute hold time the chamber was again pressurised to 1 bar with argon to reduce silicon evaporation from the surface of the infiltrated specimens and then cooled at 10 °C/min down to room temperature.

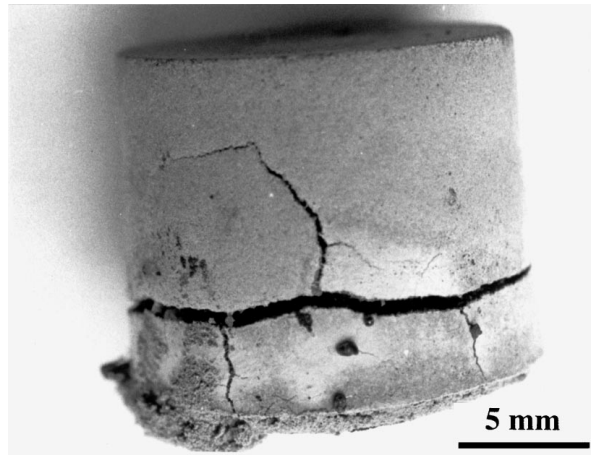

Figure 3 Macro-cracking of green compacts placed in direct contact with the melt due to rapid melt infiltration.

2.3. Characterisation of specimens

Microstructural investigation of RBSiC ceramics was conducted using scanning electron microscopy (SEM) and chemical analysis performed using X-ray diffraction (XRD) coupled with energy dispersive X-ray techniques (EDX). SEM samples were initially lapped using 25 μm diamond solution and then progressively polished with 8, 3 and 1 μm diamond slurries. Any scratches on the surface of the specimens were removed with a final polish for a few minutes on silk polishing cloths with 0.05 μm gamma alumina polish. The samples were cleaned in acetone in an ultrasonic bath for 15–30 minutes. SEM analysis was carried out on a JEOL JSM 6300 at 25 kV in the secondary electron imaging mode.

For XRD investigation, bulk samples were simply sectioned across the sample diameter. Additional preparation was not required. Examination employed a Philips PW1710 Diffractometer with Cu-Kα radiation at 35 kV and 50 mA. Peak intensities were recorded between 20–80° at a scan speed of 1.5°/min. Owing to possible texture effects in bulk samples, X-ray data was merely used to identify the phases present, rather than to establish the relative volume proportions of these respective phases.

The densities of infiltrated samples were measured in distilled water using the Archimedes density relationship.

3. Results and discussion

3.1. The infiltration process

This section details a number of experiments performed to establish the optimum processing conditions to produce well infiltrated and reacted RBSiC-$TaSi_2$ ceramics.

The first infiltrations were performed with 30 wt % graphite green compacts at 1700 °C using the theoretically calculated mass (2.22 g) and composition (28 wt % Ta) for the Si-Ta melt. The chamber was maintained at atmospheric pressure under argon for the entire process. Infiltration was attempted at 1700 °C with the preform in direct contact with the melt, but no melt penetration was observed. Previous research [1] had indicated that infiltration was possible under vacuum as well as in an inert atmosphere. Consequently experiments were repeated with the chamber evacuated to a coarse vacuum of approximately 2 mbar. In each case the compact was partially infiltrated to a depth of approximately 1.0 mm, but specimens were severely cracked at the base as indicated in Fig. 3. It is commonly accepted that too rapid a melt infiltration can cause cracking of the green preform due to the rapid evolution of heat from the exothermic Si + C reaction (ΔH_f β-SiC at 2000 °C $= -67$ kJ/mol leading to localised temperature increases of 200–300 °C [4]). Such cracks can prevent complete infiltration and reaction, and thus it was necessary to retard the rate of melt penetration. The infiltration rate may be decreased by actually separating the green preform from the melt by resting the compact on the crucible ledge a few millimetres above the melt, instead of having the compact in direct contact with the melt. In this set-up the melt has to first wick up the sides of the crucible and then penetrate the compact. This configuration prevented cracking of the specimens, and they appeared to have been completely infiltrated. However, densities were low (2.4–2.6 g/cm^3), and subsequent sectioning and microstructure examination revealed large degrees of porosity, as illustrated in Fig. 4. In addition, significant amounts of melt residue (∼30–40 wt % of the original melt) were found in the crucible well, indicating that only part of the starter melt had infiltrated the samples. As expected, powder XRD analysis of these residues revealed the presence of Si and $TaSi_2$. The relative proportions of Si and $TaSi_2$ were not determined, but their existence suggests that at the infiltration temperature of 1700 °C, the melt in the crucible became significantly enriched with Ta to cause precipitation of $TaSi_2$, thus preventing a large proportion of the melt from entering the preform. At the levels of vacuum and temperatures used, 2 mbar (∼2×10^{-3} atm) and 1700 °C, it is probable that silicon evaporates fairly readily. Evidence of silicon evaporation was the presence of powder deposits observed at a number of sites within the furnace chamber, including the furnace walls. The presence of silicon in these deposits was confirmed by EDX analysis. No Ta was detected in the powders, presumably since it has a much lower vapour pressure than Si at the infiltration temperature and is much less likely to evaporate. At 1650 °C (1923.15 K) the vapour pressures of Si and Ta are 1.71×10^{-5} atm and 1.56×10^{-14} atm [20], respectively.

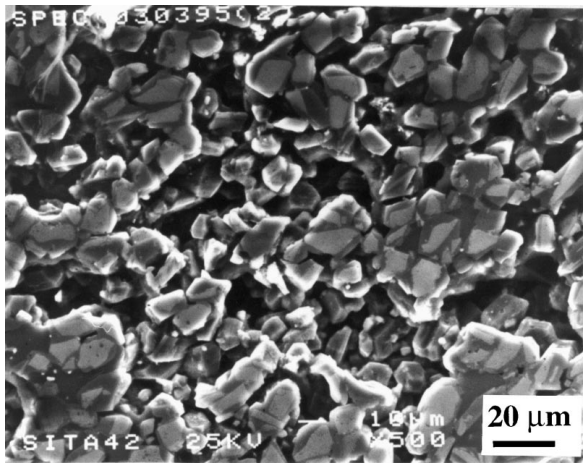

Figure 4 Significant areas of porosity in low density reacted samples, indicating poor melt penetration.

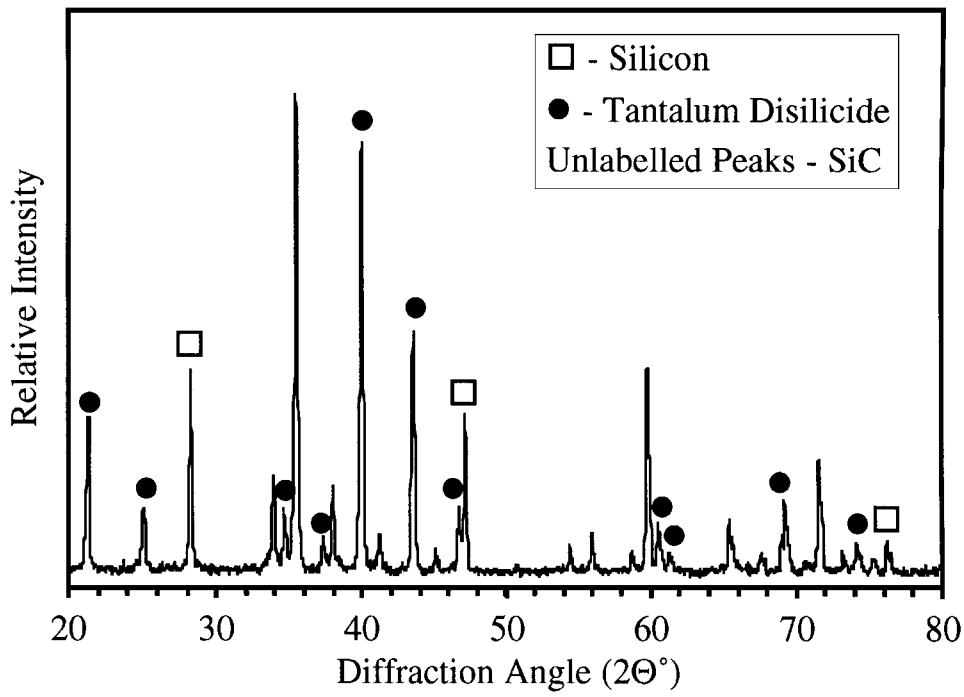

Figure 5 XRD trace of a high density RBSiC sample, indicating partial replacement of the residual Si phase with $TaSi_2$.

Loss of silicon from the melt pool in the crucible causes an enrichment of tantalum, pushing the composition closer to the Si-Ta liquidus, and causing premature precipitation of $TaSi_2$ in the crucible before infiltration of the entire compact has been achieved. With pure silicon infiltrations, the problem of silicon evaporation can be overcome by simply using excess silicon infiltrant. However with the use of Si-Ta melts, silicon evaporation will change the melt composition and can severely disrupt the infiltration process. A significant concern is that if silicon is lost by evaporation, then the melt entering the compact has a higher Ta concentration than theoretically required. This might cause premature precipitation of the silicide, which blocks off the capillaries and prevents complete infiltration and reaction of the preform. In an initial attempt to overcome the problem of silicon evaporation, the proportion of melt was increased by 50 wt %. Experiments were conducted at 1700 °C using one and a half times the theoretical melt mass (i.e. ∼3.35 g of Si-28 wt % Ta). However, the samples still exhibited large areas of porosity, and large melt residues still remained in the bottom of the crucible. Poor infiltration in all cases was believed to be the effect of silicon evaporation from the melt.

Experiments up to this point had clearly indicated that evacuation of the processing chamber was necessary to promote infiltration. However, in these experiments the chamber had been held under vacuum from 600 °C to 1700 °C. It seemed possible that the silicon may have begun to evaporate at its melting temperature of 1410 °C. With progressive Si evaporation from 1410 °C to 1700 °C the melt becomes significantly enriched in Ta, causing premature silicide precipitation in the crucible. In order to overcome this problem, the

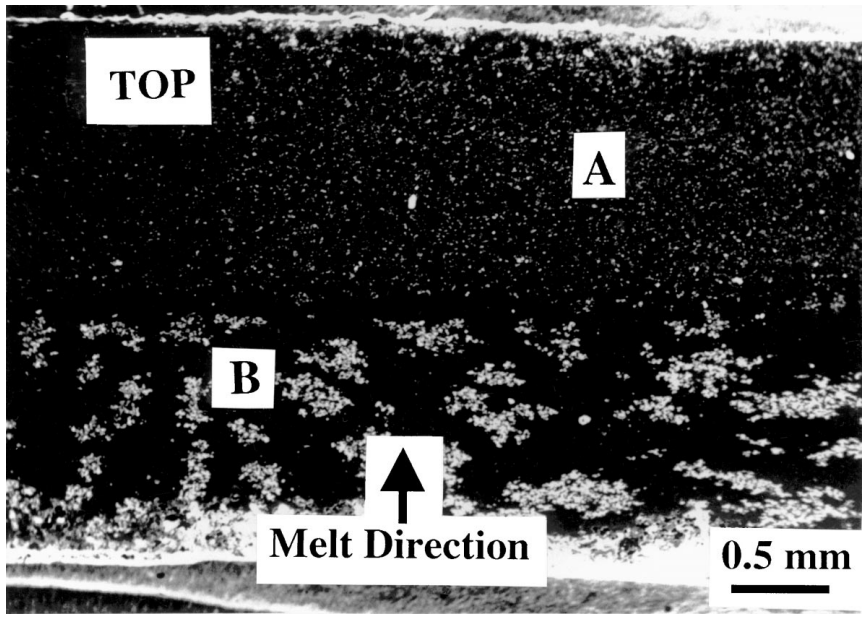

(a)

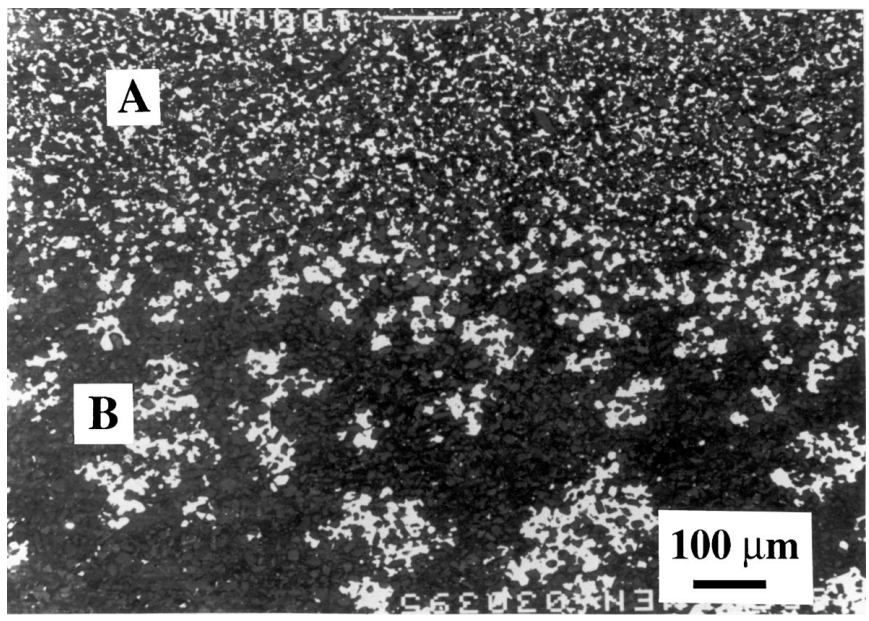

(b)

Figure 6 (a) Low magnification SEM photo of a sample sectioned vertically, indicating area **A** with a homogeneously distributed $TaSi_2$ (white) phase, and **B** with a lower $TaSi_2$ content precipitated in the form of discrete clusters. (b) Illustrating the distinct boundary between regions **A** and **B**.

furnace chamber was back-filled with argon to a pressure of 1 bar from 600 °C to 1700 °C after removal of the PEG binder phase. This reduces silicon evaporation that may occur between 1410 °C (the melting point of silicon) and the infiltration temperature. At 1700 °C, the chamber was then reevacuated to allow melt penetration of the preform. The melt composition and mass were maintained at 28 wt % Ta and 3.35 g. On bulk sample inspection after the infiltration process, samples appeared well infiltrated and exhibited densities typically ranging between 3.4–3.6 g/cm^3, with less than 2 vol % open porosity. XRD analysis indicated the presence of SiC and both residual silicon and $TaSi_2$ (Fig. 5). Solidified melt was still observed in the crucible well after infiltration but this was measured at ∼10–20 wt % of the original melt, compared to ∼30–40 wt % for previous infiltration experiments.

3.2. Microstructures and phase distribution

Subsequent sectioning and microscopic examination of the high density samples revealed some unusual characteristics of the microstructure. Fig. 6(a) is a low magnification SEM micrograph of one sample sectioned vertically. Two distinct regions of microstructure can be seen, labeled **A** and **B**. Fig. 6(b) indicates the marked boundary between these two areas. Region **A** contains a well distributed $TaSi_2$ phase (bright white), as illustrated by Fig. 7(a). Close examination of this region indicates the presence of residual silicon (black phase) in addition to the silicide phase, Fig. 7(b). However, region **B** at the base of the samples contains a $TaSi_2$ phase non-uniformly distributed in large clusters, as illustrated in Fig. 8(a). Fig. 8(b) shows a high proportion of Si (black) phase present around the $TaSi_2$. It is possible that these distinctive microstructures can provide

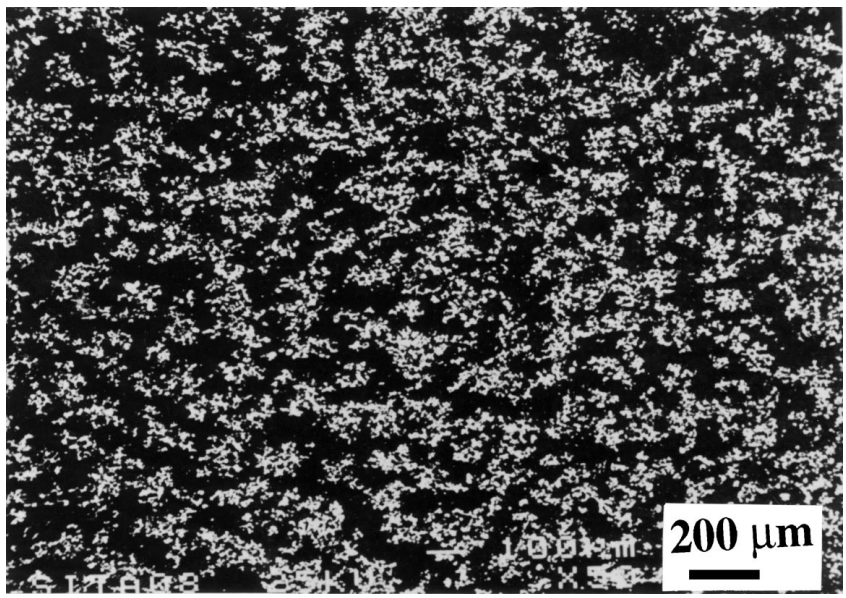

(a)

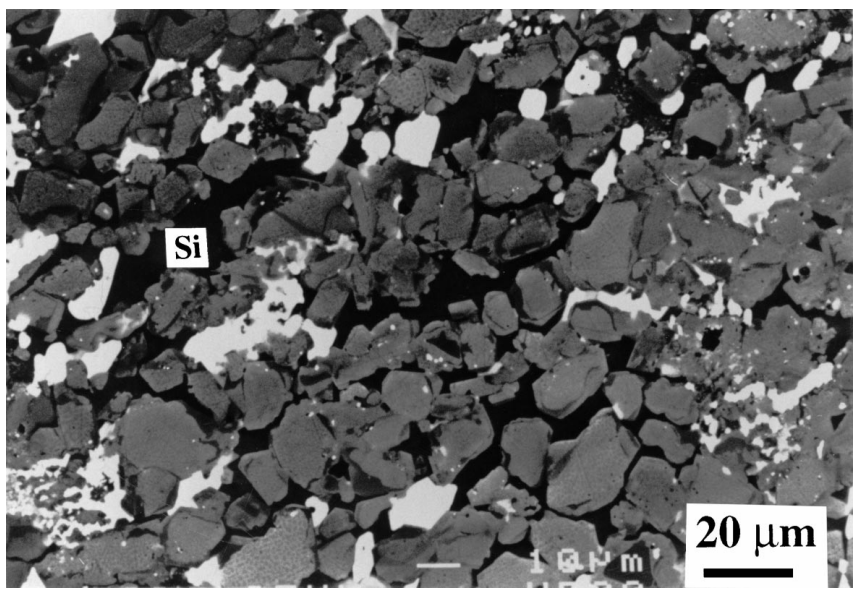

(b)

Figure 7 (a) SEM photo illustrating the high content and homogeneously dispersed $TaSi_2$ in region **A**. (b) Closer examination of region **A** indicates the presence of residual Si (black phase) in addition to the $TaSi_2$ phase. This indicates that only partial replacement of the Si phase has taken place.

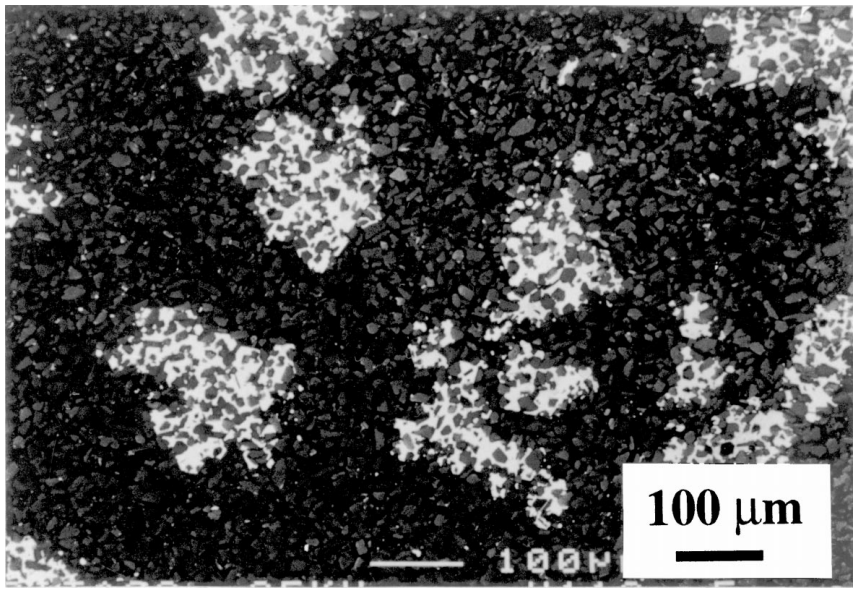

(a)

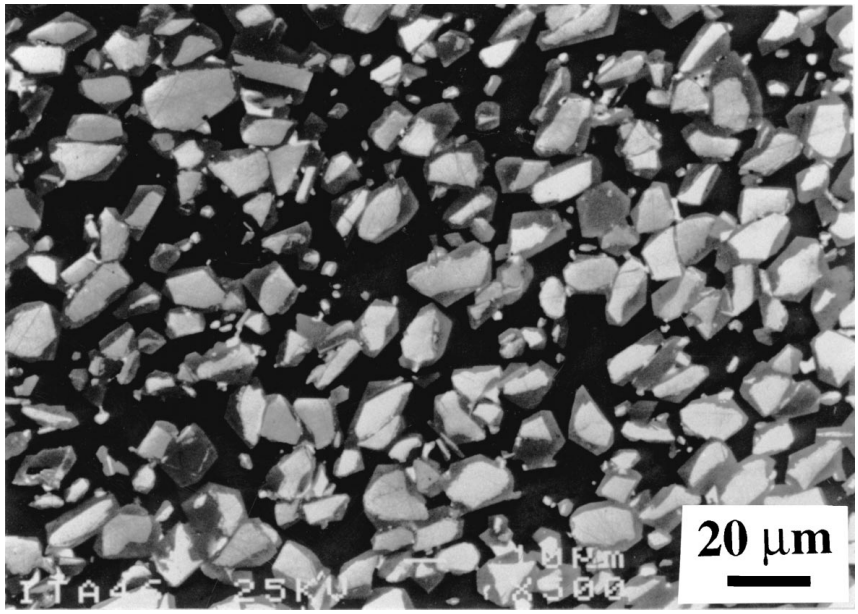

(b)

Figure 8 SEM photos (a) showing the presence of discrete $TaSi_2$ cluster precipitates at the base of the sample (region **B**), and (b) high residual Si (black phase) contents in the areas surrounding the $TaSi_2$ precipitates.

some information concerning the melt infiltration process. Regions **A** and **B** appear to have been infiltrated by melts of different composition, since they contain markedly different amounts of silicon and $TaSi_2$.

At the infiltration temperature, the chamber is evacuated to promote melt penetration of the preform. Si-Ta melt is drawn up the crucible walls by capillary force, and initially infiltrates the specimen at the edges. The edges of the preform then act as melt pools, feeding melt from the crucible into the centre of the specimen. The silicon reacts with the graphite, and the melt becomes sufficiently enriched with tantalum to cause precipitation of the $TaSi_2$ phase. This process is the basis behind reactive infiltration using alloyed silicon melts. However, the microstructure at the base of the samples suggests infiltration by a melt with a high silicon concentration. In fact, it seems most likely that infiltration of this region is by silicon vapour, which evaporates from the crucible melt pool as the chamber is evacuated. As previously discussed, much of the silicon that evaporates from the melt pool escapes to surrounding areas of the furnace chamber, but it is not unreasonable to assume that some of this silicon will actually penetrate the sample. Infiltration by silicon vapour and the Si-Ta liquid must occur concurrently. A schematic depicting the events of infiltration is shown in Fig. 9. The depth of silicon vapour infiltration is dependent on the competitive rates of both infiltrating species. Infiltration of the base region by the Si-Ta melt from the side walls of the compact is prevented because silicon vapour is simultaneously penetrating this area. Thus, the Si-Ta liquid has to move up and around the areas already infiltrated by the pure silicon infiltrant. Pure silicon infiltration of the sample will cease due to a deficiency in Si vapour, or when the Si-Ta melt has completely infiltrated the compact from the edges to

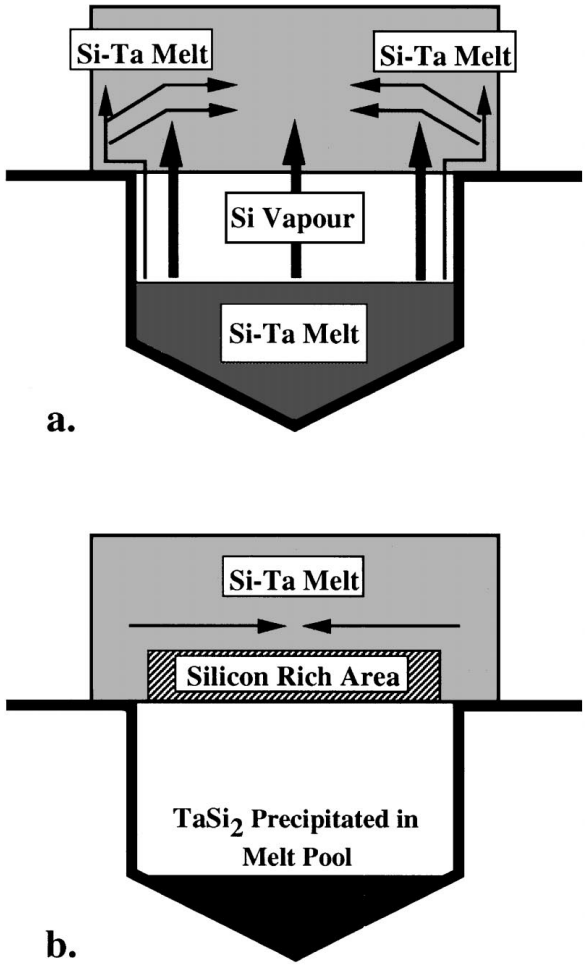

Figure 9 Schematic of hypothesised infiltration process. (a) At the start of infiltration showing concurrent Si-Ta melt penetration up the sides and into the centre of the compact and Si vapour infiltration at the base. Si vapour infiltration into the compact will cease when the Si-Ta melt penetrates across the entire diameter of the sample. (b) Towards the end of the infiltration process, indicating two areas of distinct microstructure resulting from the Si vapour and Si-Ta melt infiltrations.

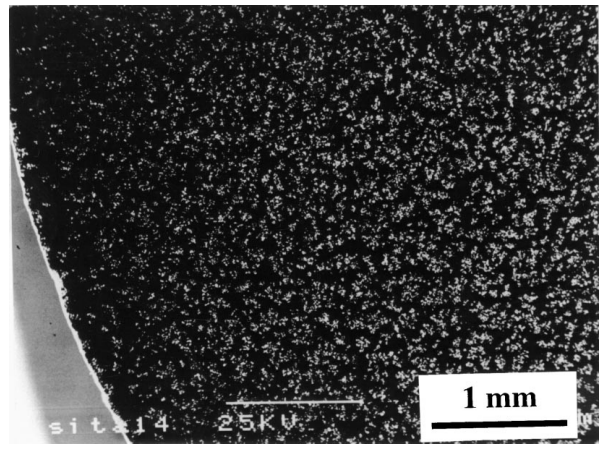

(a)

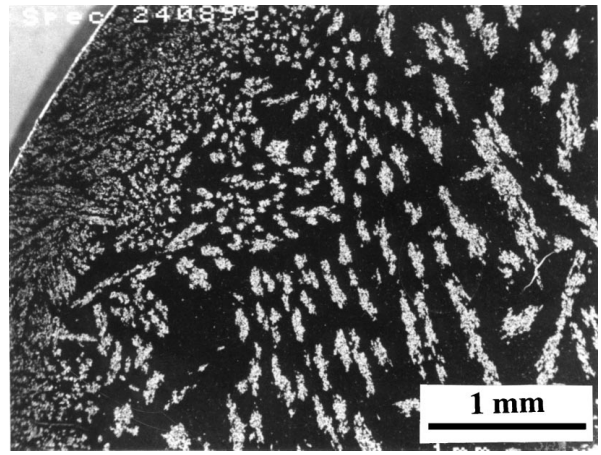

(b)

Figure 10 (a) SEM photo of a specimen sectioned across the diameter just below the top surface in region **A**. It indicates a homogeneous $TaSi_2$ phase throughout the X-section of the sample. (b) SEM photo of a sample sectioned across the diameter just above the base, region **B**, and indicating a higher proportion and more homogeneously distributed $TaSi_2$ phase at the sample edge.

the centre ahead of the silicon vapour infiltrant. Pure silicon penetration will thus be blocked by the reacted material across the diameter of the specimen, whilst the Si-Ta melt continues to infiltrate the remaining upper areas of the compact, Fig. 9.

After the infiltration process is complete, the area at the base remains filled with melt of high silicon concentration, which does not solidify until the solidification temperature of silicon (1410 °C) is approached on cooling. Thus, at the boundary between the molten silicon and the upper reacted region, silicide may redissolve in the melt and is then reprecipitated as the observed discrete clusters. If the silicide is precipitated on cooling, then the Ta has time to diffuse through the melt to precipitate at particular sites. The temperature rate of cooling of the melt influences the number of nucleation sites, and hence determines the size of the precipitates. A lower rate, which is less likely to achieve high undercoolings, induces few nucleation sites and larger precipitates.

Fig. 10(a) is a low magnification micrograph of a sample sectioned across the diameter through region **A** approximately 1 mm from the top of the sample. It indicates a uniform distribution of $TaSi_2$ throughout the cross-section. A similar section was taken at the base of the sample through region **B**, Fig. 10(b). The most significant feature is the high $TaSi_2$ content, homogeneously dispersed at the edge of the sample. This is in contrast to the centre, which exhibits a high silicon content and the discrete formation of $TaSi_2$ precipitates. This is consistent with the hypothesis that the edges of the compact are infiltrated by the Si-Ta liquid, whereas the centre of the base is penetrated by silicon vapour.

3.3. Crack formation

SEM analysis also revealed a number of cracks within the infiltrated samples. Three predominant flaw types were observed: silicide filled cracks, silicon filled cracks and unfilled cracks.

Fig. 11 illustrates examples of silicide filled cracks. They are typically 20–50 μm wide. The cracks were only observed in region **A** (the area of homogeneous silicide precipitation) and never in region **B** at the bottom of the samples. The fact that the cracks are filled with melt implies they were formed prior to or during the Si-Ta melt infiltration of the green compact, and their absence at the base of the samples further

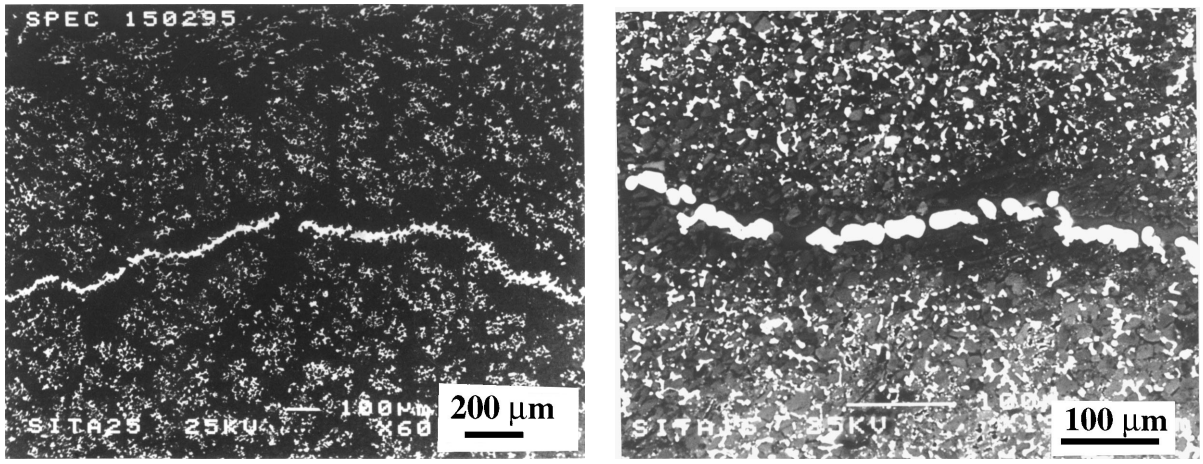

(a) (b)

Figure 11 Photos showing cracks, typically 50 μm in diameter, filled with $TaSi_2$.

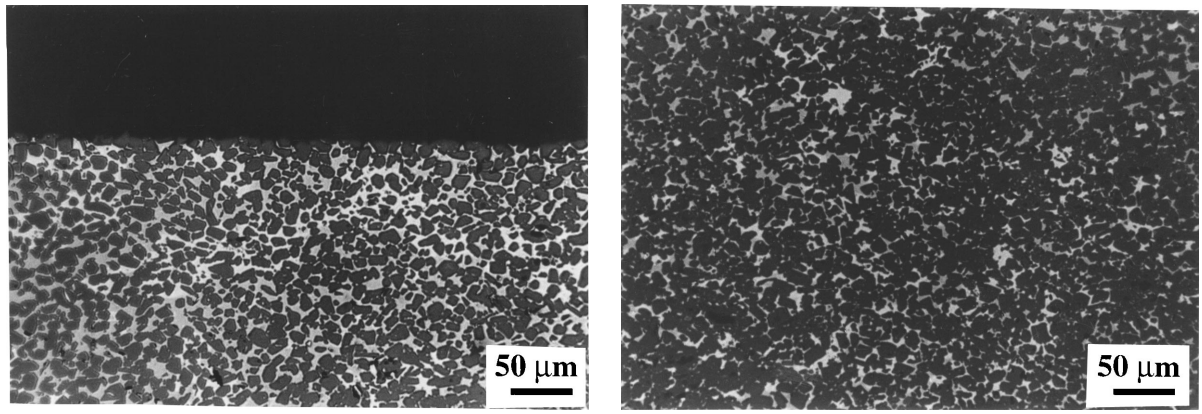

(a) (b)

Figure 12 Optical micrographs comparing SiC grain density at the edges (a) and at the centre (b) of the specimen. The variation is a consequence of poor particle compaction using uniaxial cold pressing to form the green compact.

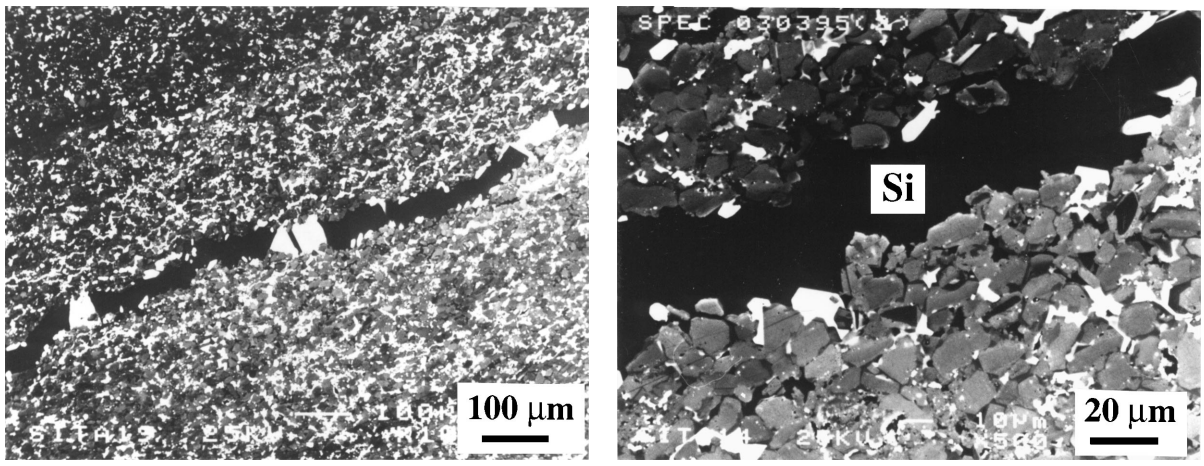

(a) (b)

Figure 13 Photos indicating cracks predominantly filled by residual Si. The presence of these cracks suggests infiltration by pure Si vapour.

indicates that Si-Ta melt did not penetrate this area of the samples. The presence of these cracks may be related to the variation in green density of the compacts. Microscopic analysis revealed the green density of the compact edges, Fig. 12(a), to be considerably lower than that of the specimen interior, Fig. 12(b). This is most likely the result of poor compaction via uniaxial cold pressing. As such, the available porosity at the centre of the preform may be lower than that theoretically required to accommodate the volume change on Si + C reaction. Thus, excessive volume expansion stresses may result in crack generation in these areas of the samples.

Fig. 13 shows silicon filled cracks. They are similar in size to the disilicide filled cracks. Their existence possibly confirms infiltration by a pure silicon

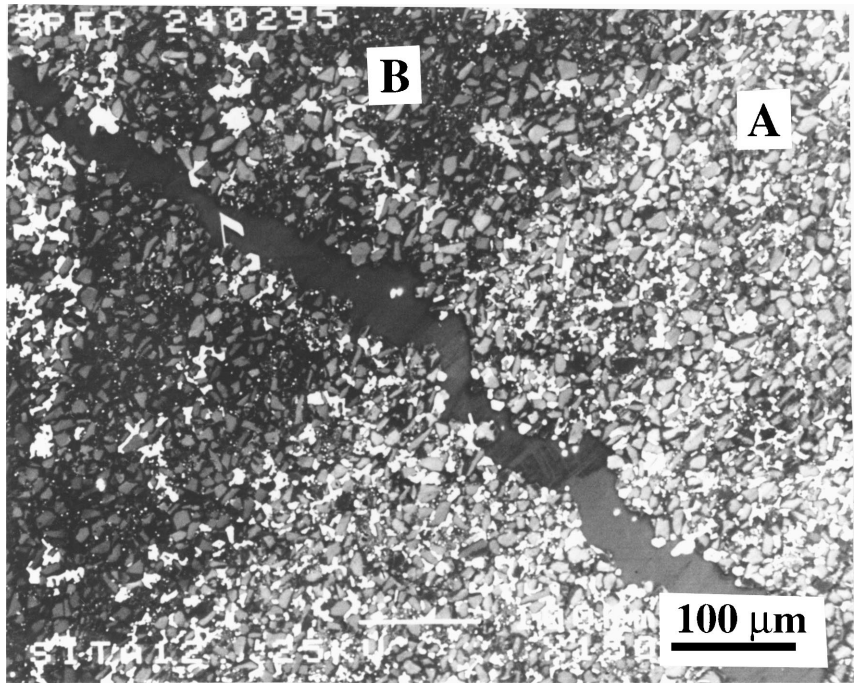

Figure 14 Indicating a Si filled crack passing vertically through the sample from region **B**, at the base, into region **A** of higher $TaSi_2$ content.

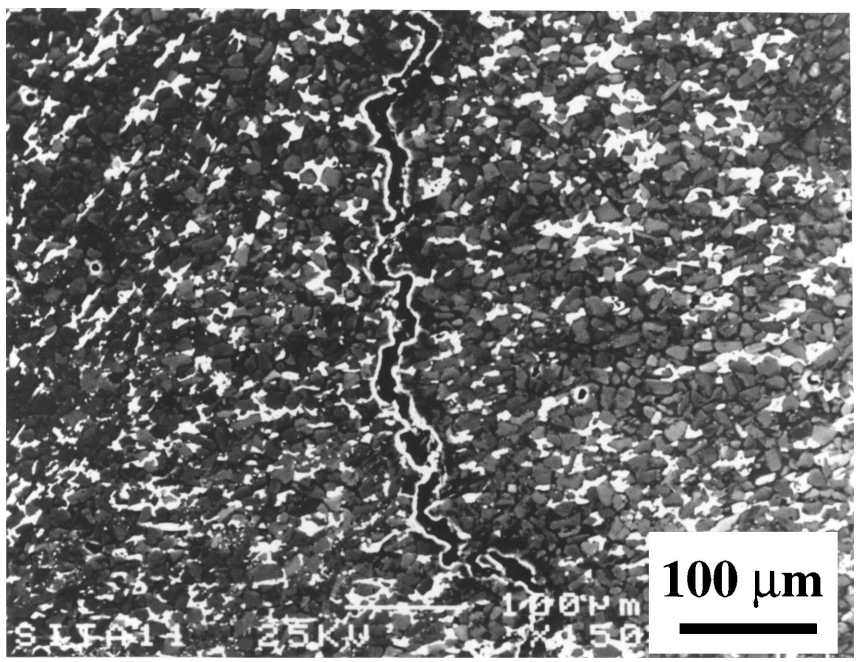

Figure 15 SEM micrograph of a crack that is not melt filled and most likely formed due to unrelieved thermal stresses or differences in the thermal expansion properties of the composite materials.

infiltrant. Unlike the silicide filled cracks, these were observed in all regions of the sample. Fig. 14 shows a silicon filled crack passing vertically through the specimen from the lower region **B** into the region of higher silicide content, region **A**. Silicon filled cracks can be formed at any time until the silicon melt pool at the bottom of the specimen solidifies, i.e. around 1400 °C. A possible explanation for these cracks could be the difference between thermal expansion coefficients of the SiC and the $TaSi_2$ phases (SiC: 4.9×10^{-6} K^{-1} [21], $TaSi_2$: 14.0×10^{-6} K^{-1} [22]). This mismatch can result in tensile stresses within the silicide material, which possibly promote cracks on cooling of the samples towards 1400 °C. These can then be filled by unsolidified silicon.

Fig. 15 shows a crack unfilled by silicon or silicide. Unfilled cracks must clearly form after infiltration and below 1410 °C (solidification temperature of silicon), since otherwise we would expect the crack to contain solidified silicon or $TaSi_2$. These are most likely formed by unrelieved thermal stresses inherent to the reaction bonding process. Short infiltration times and high temperature gradients may easily induce stresses within the material which remain unrelieved without additional thermal treatment. Messner and Chiang [13] observed such cracks in their work on RBSiC-$MoSi_2$

ceramics. In fact, their studies showed that sectioned samples had occasionally been observed to crack after a few days at room temperature, an indication of unrelieved stresses within the material. These cracks may also be the result of differences in the thermal expansion coefficients of the three phases SiC, Si and $TaSi_2$ (SiC: 4.9×10^{-6} K^{-1} [21], Si: 3.55×10^{-6} K^{-1} [21], $TaSi_2$: 14.0×10^{-6} K^{-1} [22]).

In their work, Messner and Chiang [13] observed that a reduction in the reaction rate would alleviate flaw generation within RBSiC-$MoSi_2$ materials. They also concluded that infiltration at the lowest possible temperature where the reaction rate is reduced, followed by annealing, allowed the preparation of crack-free samples. However, our experiments indicated that despite reduced infiltration temperatures, melt-filled cracks were still formed in the materials. Reduced temperatures also resulted in incomplete melt penetration of the preform and increased melt residues in the crucible.

4. Conclusion

In this study we have been able to produce composite RBSiC ceramics by an alloyed melt reactive infiltration technique. This results in the partial replacement of the lower melting Si phase by a more refractory $TaSi_2$ compound. The resulting materials exhibit high densities with virtually no detectable open porosity. However, the microstructures of these ceramics were shown to be extremely complex and exhibited some inhomogeneity, predominantly due to a phenomenon of parallel infiltration by the Si-Ta melt and pure silicon evaporating from the melt pool. It is possible that homogeneous microstructures can be produced if the problem of silicon evaporation from the melt can be resolved. It is essential that the melt composition is precisely defined, and it is necessary to ensure that the entire melt penetrates the green body. This is only possible if we prevent silicon loss from the melt by evaporation, which may require infiltrating under pressurized atmospheres, though our initial investigations indicated that this was difficult to achieve. In addition to microstructural inhomogeneities, the materials were also subject to cracking caused by a combination of rapid infiltration rates, thermal expansion differences in the composite phases and volume expansion effects on Si + C reaction. Previous work [13] has also highlighted the problems of crack formation resulting from high infiltration rates, and reported that it could be prevented by a reduction in the temperature of infiltration. Our experiments, however, did not indicate this, though other forms of crack initiation may predominate in our materials. With respect to volume expansion effects, it is absolutely necessary that green compacts be produced with a homogeneous green density, and sufficient porosity throughout the structure to allow for the volume increase on Si + C reaction. In addition, the temperature of infiltration must be sufficiently high to prevent premature precipitation of the metal disilicide and subsequently incomplete infiltration of the preform.

Acknowledgements

S.P. Simner would like to thank the Engineering and Physical Sciences Research Council (EPSRC) for provision of a graduate studentship and EA Technology for CASE support.

References

1. P. POPPER, in "Special Ceramics" (Heywood, London, 1960) p. 209.
2. P. POPPER and D. G. S. DAVIES, *Powder Metallurgy* **8** (1961) 113.
3. E. PHILLIPS and W. HUTCHINGS, AECL-3462 (1971) 1.
4. C. W. FORREST, P. KENNEDY and J. V. SHENNAN, in "Special Ceramics 5" (Heywood, London, 1972) p. 99.
5. G. R. SAWYER and T. F. PAGE, *J. Mat. Sci.* **13** (1978) 885.
6. J. N. NESS and T. F. PAGE, *J. Mat. Sci*. **21** (4) (1986) 1377.
7. C.-B. LIM and T. ISEKI, *Advanced Ceramic Materials* **3** [6] (1988) 590.
8. T. HASE, H. SUZUKI and T. ISEKI, *J. Nucl. Mater*. **59** (1976) 42.
9. L. U. OGBUJI, T. E. MITCHELL and A. H. HEUER, *J. Mat. Sci. Letts*. **14** [9] (1979) 2267.
10. W. B. HILLIG, *Am. Cer. Soc. Bull.* **73** (4) (1994) 56.
11. J. SCHLICHTING, *High Temp. High Pressures* **10** [3] (1978) 241.
12. R. P. MESSNER and Y.-M. CHIANG, *Ceram. Eng. Sci. Proc.* **9** (7–8) (1988) 1053.
13. R. P. MESSNER and Y.-M. CHIANG, *J. Amer. Ceram. Soc.* **73** (5) (1990) 1193.
14. Y.-M. CHIANG, R. P. MESSNER and C. D. TERWILLIGER, *Mater. Sci. Eng. A* **144** (1991) 63.
15. W. SCHMID, W. WRUSS, R. STROH, T. EKSTROM and B. LUX, cfi/Ber. DKG **67** (6) (1990) 245.
16. M. SINGH and D. R. BEHRENDT, *J. Mater. Res.* **9** (7) (1994) 1701.
17. Y. UMAKOSHI, in "Materials Science and Technology. A Comprehensive Treatment. Vol. 6 Plastic Deformation and Fracture of Materials" 1991.
18. S. P. SIMNER, PhD thesis. University of Oxford, England. 1996.
19. Binary Alloy Phase Diagrams Volume 3 Second Edition (ASM International, 1990) p. 3364.
20. Smithells Metals Reference Book 7th Edition (Butterworth-Heinmann, Oxford, 1992) p. 8–54.
21. Gmelin Handbook of Inorganic Chemistry 8th Edition: Silicon Supplement Volume B3 (Springer-Verlag, New York, 1986) p. 40.
22. I. ENGSTROM and B. LONNBERG, *J. Appl. Phys.* **63** [9] (1988) 4476.

Received 20 March
and accepted 15 July 1998